RESEARCH ARTICLE

Improving rubber concrete strength and toughness by plasma-induced end-of-life tire rubber surface modification

Roberto Nisticò[1] | Luca Lavagna[2,3] | Elisa A. Boot[4] | Pavlo Ivanchenko[5] |
Massimo Lorusso[6] | Federico Bosia[2] | Nicola M. Pugno[7,8] |
Domenico D'Angelo[4] | Matteo Pavese[2,3]

[1]Independent Researcher, Turin, Italy

[2]Department of Applied Science and Technology DISAT, Polytechnic of Torino, Torino, Italy

[3]National Interuniversity Consortium of Materials Science and Technology (INSTM), Florence, Italy

[4]Plasma Nano-Tech, Environment Park S.p.A., Torino, Italy

[5]Department of Chemistry and NIS Centre, University of Torino, Torino, Italy

[6]Center for Sustainable Future Technologies@Polito, Istituto Italiano di Tecnologia, Torino, Italy

[7]Laboratory of Bio-Inspired, Bionic, Nano, Meta Materials & Mechanics, Department of Civil, Environmental and Mechanical Engineering, Università di Trento, Trento, Italy

[8]School of Engineering and Materials Science, Queen Mary University of London, London, UK

Correspondence
Luca Lavagna, Department of Applied Science and Technology DISAT, Polytechnic of Torino, C.so Duca degli Abruzzi 24, 10129 Torino, Italy.
Email: luca.lavagna@polito.it

Abstract

This study evaluates the effectiveness of using different plasma treatments to favor the compatibility between rubber and a cement matrix in composites, thus leading to a different surface reactivity of the rubber component. Plasma-treated rubbers were introduced into two different types of concrete. Mechanical tests highlighted that Portland concrete composites filled with N_2/H_2 plasma-treated rubber had increased flexural strength, toughness, and compression strength compared to composites containing untreated rubber. A scaling law is also proposed to qualitatively discriminate between related effects due to topological/roughness or intrinsic/chemical adhesion modifications. Plasma treatment can improve both intrinsic adhesion and roughness of the rubber–cement interface and thus the overall concrete strength and toughness.
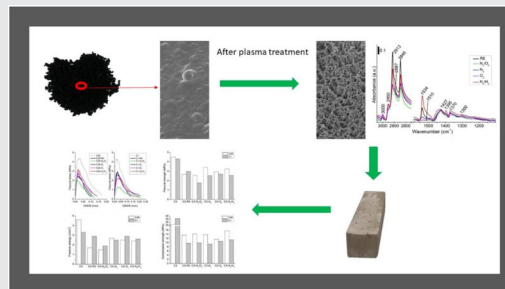
KEYWORDS

composite materials, concrete, mechanical properties, plasma treatments, rubber, surface modifications

1 | INTRODUCTION

In recent years, the possibility to reuse end-of-life rubber from waste tires to replace the aggregate fraction in concrete has caught the attention of researchers worldwide due to the high added value in terms of both economic/environmental sustainability and functional properties.[1–10] From the sustainability viewpoint (and according to the principles of the circular economy), the valorization of end-of-life materials for manufacturing

novel products or reducing the production costs of existing materials (thus overcoming the concept of waste, turning it into a resource) is a technical solution that guarantees a significant step forward in the direction of sustainable development.[11,12] In this context, the scientific literature provides several examples of waste valorization for the production of composite materials to be exploited in advanced applications.[13–24] Among the different types of waste, crumb rubber from scrapped vehicle tires has become very attractive due to the high volumes generated from cars and other vehicles (European consumption of tires per year is ca. 3.2 million tons).[1,25,26] As reported in the literature,[27] the composition of tires is primarily organic (rubber/elastomers ca. 48%, and carbon black ca. 22%), with an inorganic fraction (metal ca. 15%, zinc oxide ca. 1%, and sulfur ca. 1%) together with textiles (ca. 5%) and other additives (ca. 8%).[28] After the removal of the metallic ring, end-of-life tires are properly reprocessed (by means of several milling techniques) to obtain materials of various sizes and shapes, such as rubber chips (whose size is in the 20–50 mm range), rubber granulate (in the 1–20 mm range), rubber powder (less than about 1 mm), and textiles (in the shape of both short fibers and/or strips).[1]

From the functional viewpoint, the introduction of reprocessed tires to partially replace the coarse and/or fine aggregate fraction in concrete, thus forming rubber concrete composites, is an attractive technological solution exploitable in the construction industry and civil engineering, mostly for the development of sustainable shock/impact/vibration absorbers, heat/sound insulators, or lightweight parts.[29] Obviously, these properties are unusual for concrete and are, in principle, proportional to the rubber content. Unfortunately, as highlighted by Sgobba et al.,[30] one of the main concerns of these composite materials is the poor interfacial adhesion between the two components (namely, the inorganic cement paste and the organic elastomeric component), which causes significant degradation in terms of mechanical properties, and consequently a considerable limitation in the effective exploitability of the rubber. To overcome this interfacial issue, several specific physicochemical treatments have been suggested in the literature (e.g., surface roughening, immersion in either NaOH or H_2SO_4)[2,31–33] as well as the introduction of additives (e.g., pozzolana)[34] in the formulation.

Quite recently, plasma-induced radiation treatments have gained great interest due to their ability to alter only the surface properties of materials without compromising the bulk characteristics.[35–37] Plasma radiation consists of an electrically neutral ionized gas mixture so that it can be considered a clean (and environment friendly) technology due to the absence of any hazardous reactants. Depending on the chemical (reactive) species constituting the plasma phase, several different surface effects can be induced by performing plasma treatments: surface cleaning, roughness increments, radical formation (i.e., chemical reactions), or polymerization (i.e., coating deposition).[38] In particular, plasma treatments were successfully exploited for enhancing the surface wettability and interfacial adhesive response of polymeric fibers by either including oxygen-containing functional groups[39–41] or depositing a coating via plasma polymerization.[42,43] Radiation-induced surface modification of tire rubber has previously been performed by Zhang et al.[44] by means of an atmospheric plasma (air-gas mixture), registering an increment of the interfacial adhesion of the treated tire rubber, thanks to the creation of carbon–carbon double bonds and oxygen-containing functionalities.

In this study, four different plasma treatments (i.e., N_2/H_2, N_2, N_2/O_2, O_2) were used to modify the surface compatibility of end-of-life tire rubber with cement paste. Subsequently, after a thorough physicochemical characterization necessary to understand the plasma-induced chemical modifications, plasma-treated tire rubber was used to produce rubber concrete by partially replacing the aggregate fraction. Two different types of matrices were investigated: (i) Portland cement Type II/B (curing: 28 days, 20°C) and (ii) Class G cement (curing: 24 h, 85°C), widely used in either structural applications for the building industry or for the oil industry, respectively.

2 | EXPERIMENTAL SECTION

2.1 | Materials

End-of-life tire rubber was obtained from the TerniEnergia S.p.A. treatment plant located in Narni (Terni, Italy). The end-of-life tire treatment is a multistep procedure.[45] Tires were initially reduced in the shape of chips (size: 50–100 mm). Rubber chips were further milled and the residual metallic steel removed through the action of an external magnet. Subsequently, several milling and separation steps were realized by the TerniEnergia S.p.A. to finally obtain a medium-sized rubber granulate (size: 0.8–2.5 mm, Figure 1).

2.2 | Plasma apparatus and plasma treatment conditions

A plasma-enhanced chemical vapor deposition PICO type from Diener Electronics GmbH was employed to perform the plasma experimental tests.
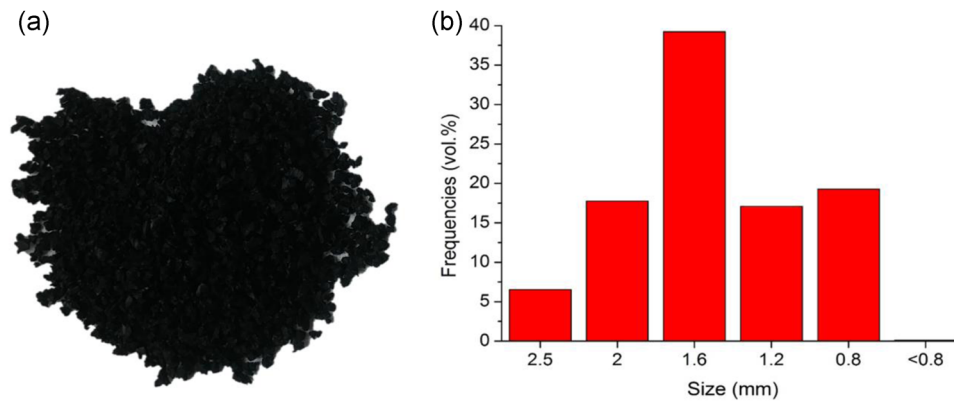
FIGURE 1 (a) Medium-sized rubber granulate used in this study. (b) Overall size distribution of the medium-size rubber granulate

The PICO plasma system type consists of a vacuum chamber (chamber design cylindrical with dimensions: diameter 150 mm; T, 320 mm), a generator (40 kHz, 0–200 W), a pumping system (Pfeiffer DUO 2.5C—2.5 m^3), a standard electrode type A (aluminum), and a gas supply channel (1 pcs. stainless steel needle valve).

The process begins by pumping the PICO chamber down to a pressure lower than 5 mbar through the first line to evacuate the atmospheric air. When low pressure is achieved, the second line is switched on, and the gate valve is closed. The pressure is then increased with the inflow of the process gas up to the final pressure of the target process. After pressure stabilization, the radiofrequency (RF) power is turned on at the desired power level, and at plasma ignition, the process begins. When the treatment time ends, the RF power is turned off automatically, the second line pumping is closed and the gate valve is opened.

Discharge operating conditions include the flow rate of gas, power, and time exposure time. The tests were carried out with four different gas combinations: N_2/H_2 (nitrogen 96%–hydrogen 4%), pure N_2, N_2/O_2 (nitrogen 80%–oxygen 20%) and pure O_2. In all experiments, the exposure time was 5 min of treatment repeated twice with an interval of 1 min, to avoid excessive heating of the rubber. The first process started with 200 W of power, 20 sccm of gas mixture N_2/H_2, and the pressure was stabilized to 1.2 mbar. During these experiments, the process temperature was 40°C. The second process was performed using the same power condition, and pure nitrogen at an operating pressure of 1.4 mbar. The third process was performed using the nitrogen–oxygen mixture (80%–20%) at an operating pressure of 1.3 mbar. The fourth experiment was performed using pure oxygen at an operating pressure of 1.6 mbar.

2.3 | Preparation of rubber concrete samples

Concrete composites were prepared by mixing the cement paste with standard sand (Societe Nouvelle Du Littoral) UNI EN 196-1:2005 and rubber granulate. The concrete paste, prepared at a water-to-cement (w/c) ratio of 0.5, was then poured into prismatic molds (80 × 20 × 20 mm in size) and properly cured. Two different cement types were used for composite preparation: (i) a Portland cement Type II/B (Lauriano 42.5R) UNI EN 197/1 cured first for 24 h at 20°C in an environment with 100% relative humidity and then for other 27 days at 20°C immersed in tap water, and (ii) an American Petroleum Institute (API) oil-well cement Class G (Lafarge North America) cured for 24 h at 85°C and 100% relative humidity.

Being a cement paste containing sand the most correct definition would be mortar, however, in a broad sense, mortar is usually denoted as concrete in the literature. For simplicity, the term concrete was adopted in the text to avoid misunderstandings.

The replacement of aggregate was 15 vol% with respect to the total aggregate volume for all rubber concrete samples. At the end of the curing time, specimens were notched by means of a Remet type TR100S abrasive cutter with a 2 mm thick diamond cut-off wheel, realizing a 5 mm deep U-shaped notch.

Composite samples were coded with the following acronym: CX-Y; where X refers to the curing time (expressed in days) of the concrete paste (namely, 28 for Portland cement and 1 for Class G cement), and Y refers to the type of rubber introduced: R0 (for untreated rubber), N/H (rubber treated with N_2/H_2 plasma), N (rubber treated with pure N_2 plasma), N/O (rubber treated with air plasma), and O (rubber treated with pure O_2 plasma). Concrete samples without rubber were indicated as C28

when cured for 28 days at room temperature, whereas the ones cured for 24 h at 85°C were indicated as C1

2.4 | Physicochemical and mechanical characterization

Optical emission spectroscopy (OES) was performed by means of an Ocean Optic spectrometer LIBS2500 2plus-optic probe QP600-2-SR/BX, using integration times (optical scan) of 100 ms.

Infrared (IR) spectra of the rubber samples were collected in attenuated total reflectance (ATR) mode (Golden Gate single-reflection ATR cell with ZnSe lenses, by Specac equipped with a diamond window) using a Bruker Vector 22 spectrometer (resolution 4 cm^{-1}; detector MCT). Each sample was measured at least five times to verify the homogeneity of plasma treatments across the sample. All spectra resulted from an average of 250 scans. The elaboration of the spectra was carried out by exploiting OPUS 5.0 Spectroscopy Software by Bruker Optik GmbH.

Field-emission scanning electron microscopy (FESEM) micrographs were collected by means of a FESEM Zeiss Merlin. Morphologic characterization was performed by depositing the rubber on a sample holder, drying and analyzing different areas. Before performing the measurements, a thin layer of Cr was deposited by sputtering on the samples, to avoid any charging effects.

Scanning probe microscopy (SPM) was performed using a Hysitron TI 950 Tribo Indenter. Scanning was performed on the sample at a scan rate of 1 Hz with a tip velocity of 10 μm·s^{-1} using a Berkovich tip with a radius of 150 nm. The average roughness (R_a) was calculated on a scan size of 10×10 μm using Gwyddion, a modular open-source program for SPM data visualization and analysis.

Flexural mechanical tests of the concrete composites were performed in a three-point bending configuration (ASTM C348) in crack mouth opening displacement (CMOD) on notched specimens of size $80 \times 20 \times 20$ mm (notch width: 2 mm, depth: 5 mm).[46,47] The specimens were tested with a single-column Zwick-Line z050 testing machine with a 1 kN load cell. CMOD was controlled by fixing the CMOD rate of 0.005 mm·min^{-1} using an extensometer placed between the two sides of the notch. The distance between the supports was fixed at 65 mm. Mechanical tests were realized on at least three specimens per sample. The flexural strength was calculated by applying the standard formula for unnotched bending tests (considering the nominal thickness thus of the unnotched cross-sectional area), whereas the fracture energy (measured in J/cm^2) was calculated by integrating

the force–CMOD curves following the procedure prescribed by the JCI-S-001-2003 standard and then normalizing on the actual thus notched cross-sectional area.

The compression strength of the concrete composites was measured on cubic specimens $20 \times 20 \times 20$ mm in size[46,47] obtained from the prisms used for bending tests after failure. The specimens were tested with a single-column Zwick-Line z050 testing machine with a 50 kN load cell. The tests were performed at a fixed displacement rate of 0.1 mm·min^{-1}. Mechanical tests were realized on at least three specimens per sample.

3 | RESULTS AND DISCUSSION

3.1 | Plasma-induced modification of tire rubber

To investigate the degree of ionization and dissociation within the glow discharge, OES was used, and the intensities of the molecular, atomic, and ionic species that were observed in the plasma were measured. To minimize air contamination, the chamber was evacuated three times and then filled with the process gas. Figure 2 shows the optical spectra of the N_2/O_2 (mixture 80:20), N_2, O_2, N_2/H_2 (mixture 95:5). In the spectra acquired using the N_2/O_2 mixture (Figure 2a), in addition to the emission corresponding to an N_2 second positive system and N_2^+ first negative system, it is also possible to observe the signals corresponding to an N–O γ system at 247.0 ($A^2\Sigma^+ \rightarrow X^2\Pi$ transition), and two additional lines at 777.0 and 844.0 nm, which are related to the electron transition of oxygen atoms O* from $3p^5P$ to $3s^5S$ and from $3p^3P$ to $3s^3S$. As shown in Figure 2b, in the pure N_2 discharge, the main contribution to emission from this region corresponds to the N_2 second positive system (2^+) and the N_2^+ first negative system (1^-). Peaks representing the N_2 second positive system (315.9, 336.7, 357.6, 380.8 nm) and the N_2^+ first negative system (391.1, 427.8, 470.9 nm) are observed. Figure 2c shows the pure O_2 discharge: the main contributions are two lines at 777.0 and 844.0 nm, which are related to the electron transition of oxygen atoms O* from $3p^5P$ to $3s^5S$ and from $3p^3P$ to $3s^3S$. There are also two low-intensity additional signals (393.0 and 436.0 nm) related to the electron transition of oxygen atoms O* and a low signal at 336.7 nm corresponding to the N_2 second positive system. The low intensity of this signal with respect to that of the oxygen species indicates that small amounts of nitrogen atoms remain in the chamber. In the spectra collected in the N_2/H_2 mixture discharge (Figure 2d), the main contribution to emission from the same region corresponds to both 1^- and 2^+ systems of nitrogen and H_α, N–H
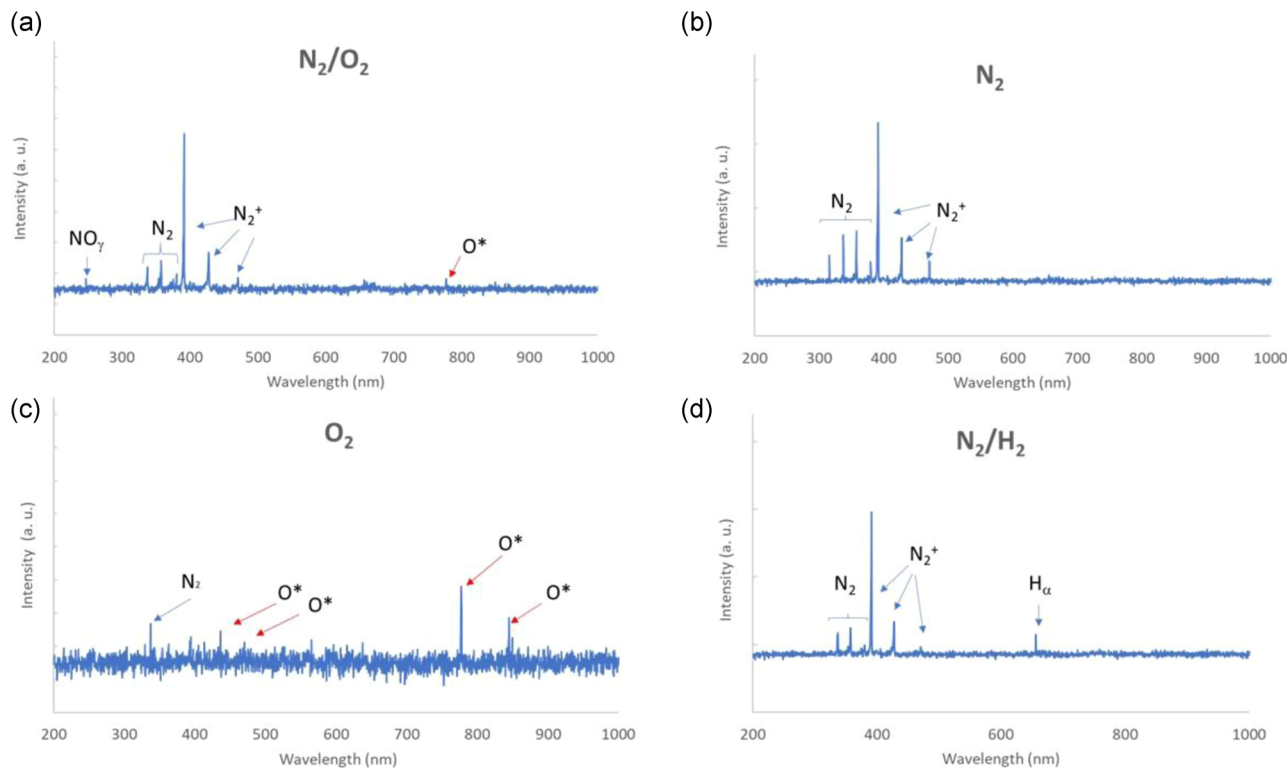
FIGURE 2 Optical emission spectra in the 0–1200 nm range relative to N_2/O_2 (a), N_2 (b), O_2 (c), and N_2/H_2 (d) plasmas

transitions. Although only the atomic hydrogen lines at 656.3 nm are observed in the nitrogen–hydrogen plasma spectra, the presence of hydrogen can be highlighted by the shoulder to wavelengths in the nitrogen band at 336.7 nm. This shoulder corresponds to the N–H band at 336.3 nm. Peaks representing the N_2 second positive system (336.7, 357.6, 380.8), N_2^+ first negative system (391.1, 427.8, 470.9), N–H transition $A^3\Pi \rightarrow X^2\Sigma^-$ (336.3) and H_α (656.3) are observed.

The IR–ATR spectra of all the rubber samples in a high-frequency region (Figure 3) exhibit the typical profile for systems containing a set of C–H oscillators. The details related to the assignment of the bands present in the spectra are described below. Overall, regardless of the treatment, the spectra exhibit profiles similar to the pristine sample with slight specific variations for each case. In comparison with the spectrum of the pristine rubber, the N_2/H_2 plasma treatment resulted in the vanishing of the signal at 3000 cm^{-1} (due to vinyl νCH) and at 2887 cm^{-1} (due possibly to aldehydes; the associated aldehyde band in the 1700–1750 cm^{-1} range is not sufficiently intense to be visible in the IR spectrum); also, a decrease in the intensity of signals at 2913 and 2846 cm^{-1} (due to $\nu_{asym}CH_2$ and $\nu_{sym}CH_2$) is observed, while the band at 2950 cm^{-1} (due to νCH_3) remains after the modifications. Further, plasma treatments in N_2, O_2, and air (N_2/O_2) resulted in a significant decrease of all

the main bands in this region except for the components at 2887 and 3000 cm^{-1}. In particular, the 3000 cm^{-1} band increased after N_2 and O_2 treatments and remained almost unchanged after the air (N_2/O_2) treatment. Instead, the 2887 cm^{-1} band increased with O_2 treatment and remained unchanged for N_2 and air treatments. Interestingly, plasma treatment in an N_2 or O_2 atmosphere resulted not only in a decrease of the intensity of the
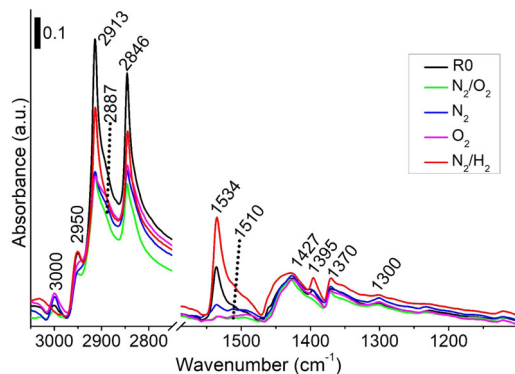

FIGURE 3 Attenuated total reflectance–Fourier-transform infrared spectra in the 3500–1100 cm^{-1} range of untreated rubber R0 (black curve) compared with plasma-treated rubber: N_2/H_2 (red curve), N_2 (blue curve), N_2/O_2 (green curve), and O_2 (magenta curve)

bands at 2913 and 2846 cm^{-1} but also in a noticeable change of their relative intensities.

The fingerprint region of the pristine rubber spectrum is characterized by a sharp intense signal at 1534 cm^{-1} with a noticeable shoulder at ca. 1510 cm^{-1} attributable to N-containing functionalities, a band at 1427 cm^{-1} due to δCH_3, a band at 1395 cm^{-1} is due to $\nu S=O$, a band at 1370 cm^{-1} due to methylene δCH and a low-intensity band at 1300 cm^{-1} due to skeletal C–C vibrations. The plasma treatment in an N_2/H_2 atmosphere resulted in a significant (almost double) increase of the intensity of the signal at 1534 cm^{-1}, along with an increase of the bands at 1395 and at 1370 cm^{-1}, accompanied by a considerable broadening of the band at 1427 cm^{-1}. On the contrary, the N_2, O_2, and air (N_2/O_2) plasma treatments caused a dramatic decrease of both the band at 1534 cm^{-1} and the component at 1395 cm^{-1}.

In the treatment with a pure nitrogen plasma, the signals related to the formation and recombination of the N_2^+ species are present, as observed by OES in Figure 2. Indeed, the hypothesized reaction mechanism, in this case, involves the formation of the N_2^+ species, which accelerates through the ion sheath and, on the way to the surface substrate, generates energetic N_2 by charge exchange collisions. This phenomenon induces a series of reactions on the surface that lead to cross-linking reactions, and reactions leading to the loss of the functional groups, in particular those based on N and O, which are most affected by the effects of polarization.[48] In this case, there is a decrease in the intensity of the signals at 1534 and 1510 cm^{-1}. The presence of energetic N_2 leads, however, to a small increase of surface roughness, as shown in Figure 4.

The effect of the N_2/H_2 mixture is different as the presence of hydrogen increases the probability of dissociative sticking of N_2 at the cathode surface by decreasing the work function of the substrate.[49] Optical spectroscopy shows the signals of the species involved in this reaction mechanism very well. Consequently, the effect on the sample surface is a reduction of the signal at 3000 cm^{-1} (addition of hydrogen) and an increase of the signals at 1534 and 1510 cm^{-1}. Therefore, the treatment of rubber with N_2/H_2 mixture plasma facilitates the formation of N functional groups to the surface. Nevertheless, the low-energy content of the discharge does not allow an efficient chemical–physical effect on these groups that remain almost unchanged, showing an increase in the signal as a whole.

Instead, the treatment with the N_2/O_2 mixture produces partial oxidation of the rubber, which has the effect of reducing the signals at 1534, 1510, 2913, and 2864 cm^{-1}. Reductions in the bands at 2913 and 2864 cm^{-1} were associated with aliphatic breaking and aldehyde C–H group bonds (CH, CH_2, and CH_3 groups) caused by rubber oxidation,[50] while the band at 2887 cm^{-1} is still visible. The uniform plasma distribution typical of an N_2/O_2 mixture generates a homogeneous smoothing of the surface, whose roughness remains similar to the untreated rubber.

When the rubber is exposed to pure oxygen discharge, oxidation is produced on the rubber surface, causing the disappearance of N functional groups and the reduction of the bands at 2913 and 2864 cm^{-1}, as in the case of N_2/O_2 mixture. Also, the increase in the band at 2887 cm^{-1} is observed, due to added aldehyde-type functionalities, and the band at 3000 cm^{-1} increases too, probably due to hydrogen elimination. At the same time, the presence of a high quantity of highly energetic oxygen-based species (radical oxygen at 777.0 nm) causes a considerable local etching effect on the surface, leading to a considerable increase of roughness (Figure 4).
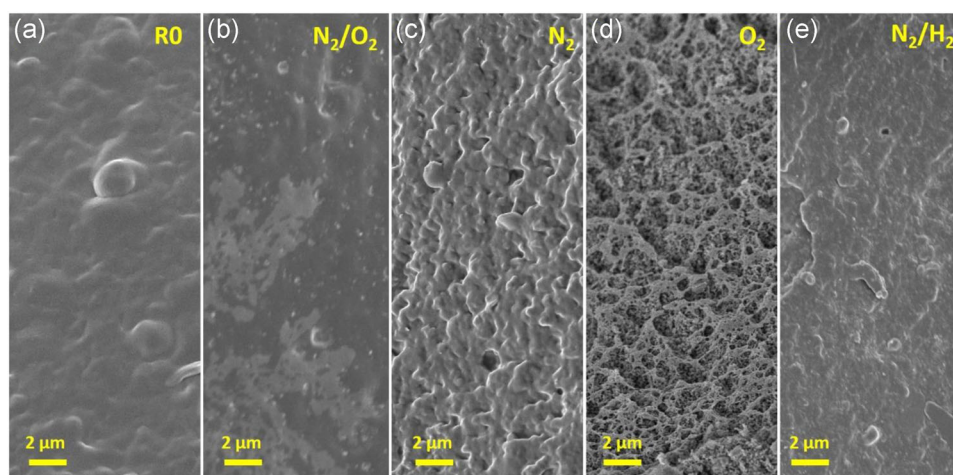

FIGURE 4 Field-emission scanning electron microscopy micrographs of untreated rubber (R0) (a) and plasma-treated ones (N_2/O_2 (b), N_2 (c), O_2 (d), and N_2/H_2 (e)). All images were collected at the same magnification
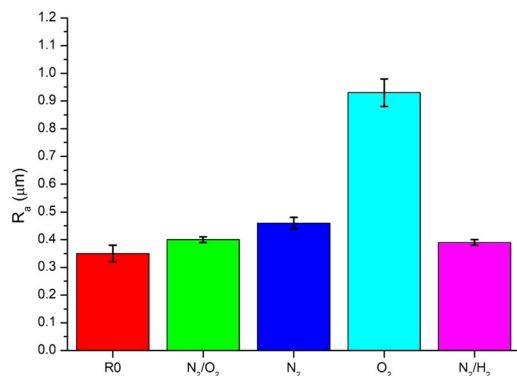
FIGURE 5 Roughness (R_a) of samples measured through scanning probe microscopy: plasma treatment increases the roughness

As already discussed, the plasma modifies the surface roughness of the rubber, and this effect is shown in Figure 4, where the rubber surface is shown, as observed by FESEM. In particular, the treatments with N_2/O_2 and N_2/H_2 plasmas seem to have only a slight effect on the surface structure of the rubber, while the treatment with O_2 plasma creates a very rough structure. In the case of the plasma made with N_2, there is a limited increase of surface roughness. To measure the induced roughness, SPM was performed and the results are presented in Figure 5.

The measured R_a of the untreated rubber sample (R0) is $0.35 \pm 0.03\,\mu m$. The sample treated with air plasma (N_2/O_2) and the sample treated with N_2/H_2 plasma have similar roughness, only slightly greater than the one of the rubber without plasma treatment, respectively, 0.40 ± 0.01 and $0.39 \pm 0.01\,\mu m$. The R_a of the sample treated with N_2 plasma is significantly greater than that of rubber without a plasma treatment ($0.46 \pm 0.02\,\mu m$). The sample treated in O_2 plasma displays the largest roughness value ($0.93 \pm 0.05\,\mu m$). The SPM analysis results confirm the conclusions derived from FESEM micrographs.

Thus, by coupling optical emission and IR spectroscopic data with SEM observation and SPM roughness measurements, we can conclude that the treatment with N_2/H_2 leads to a marginal increase of roughness but produces N-containing functional groups. The treatment with nitrogen, due to the dynamics described above, brings to an increase of the roughness of the rubber, small but higher than in the case of N_2/H_2 mixture, but leads to a reduction of nitrogen-based functionalities. The treatment with the N_2/O_2 mixture or with pure O_2 reduces the content of the N-based functionalities; while the N_2/O_2 mixture has almost no effect on roughness, due to a diffuse etching effect on the surface, the treatment with pure O_2 leads to a considerable increase in

roughness, with the formation of a porous surface structure.

3.2 | Mechanical performance of rubber-containing concrete

Figure 6 and Table 2 report the results of mechanical tests performed on concrete (C28 and C1) and on rubber concrete. In general, samples containing rubber exhibit smaller flexural strength if compared to pristine concrete. This behavior is probably due to the intrinsic rubber mechanical properties and to the small interface strength.[30] However, encouraging responses were obtained from the composites containing plasma-treated rubber, showing a possible increment in terms of mechanical performance if compared to the reference rubber concrete containing untreated rubber (Figure 6).

In particular, bending tests performed on the C28 series revealed that composites containing plasma-treated rubber display better performance with respect to those containing untreated rubber (the only exception is the composite filled with N_2/O_2 plasma-treated rubber, C28-N_2/O_2, whose flexural strength is analogous to the untreated sample). Among the different considered treatments, those generating the best mechanical properties in rubber-filled concrete were "reducing" plasmas, namely N_2/H_2 (C28-N_2/H_2) and N_2 (C28-N_2). On the contrary, bending tests performed on the C1 series showed that in all cases, composites containing plasma-treated rubber had worse a performance compared to those containing pristine rubber. These effects are probably attributable to the harsher conditions (higher temperature) necessary for curing the C1 concrete. The high curing temperature can affect the stability of the plasma-induced chemical modifications and consequently quench their beneficial effect.

The effectiveness of plasma treatments is even more evident when considering the composite fracture energy (Figure 6c). As found previously for flexural strength, fracture energy values for the C28 series reveal that an improvement of performance is obtained for most of the plasma-treated composites (the only exception is again the N_2/O_2 composite). This is encouraging as it indicates that the plasma treatments induce a better interfacial adhesion between rubber and cement matrix, inhibiting crack propagation. In the C1 series, a high level of uncertainty is observed in the data (as reported in Table 3), so that it is difficult to draw definitive conclusions about the effect of the plasma treatment. However, the data suggest that again, probably due to the effect of high curing temperature, the fracture energy of samples containing plasma-treated rubber is smaller than in the case
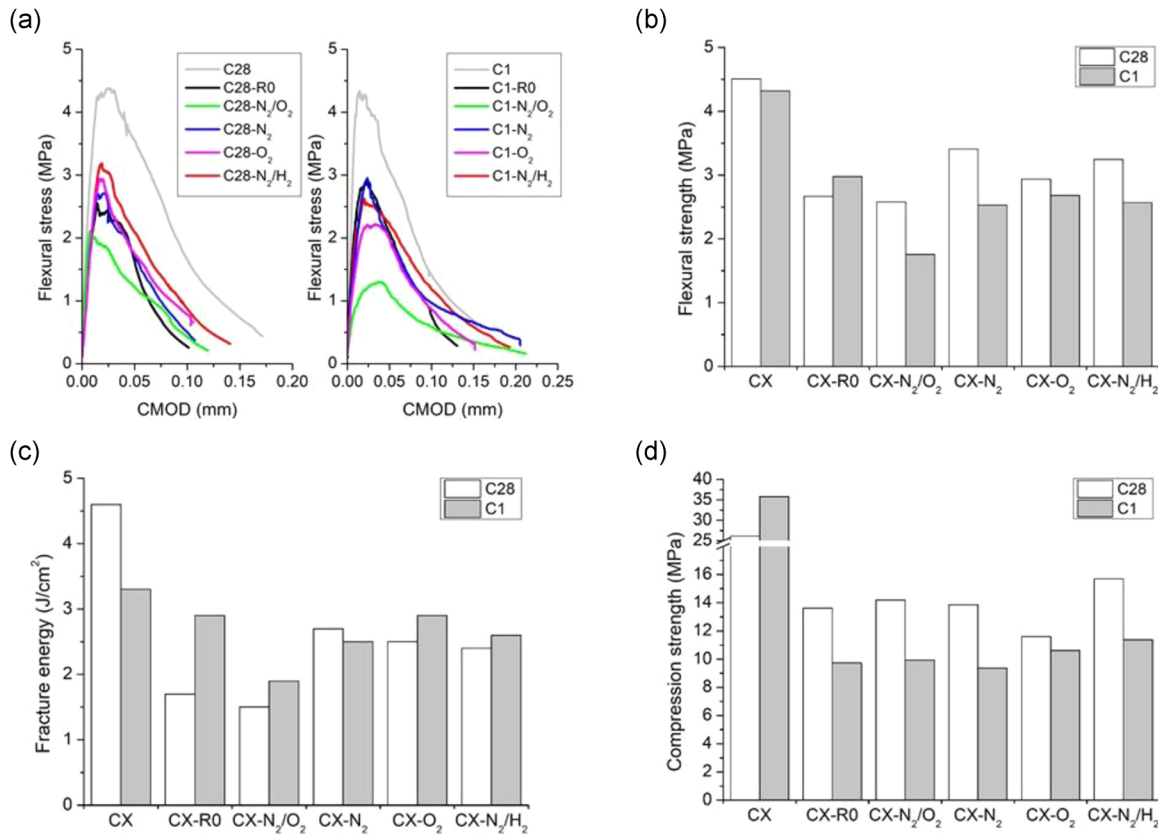
FIGURE 6 Mechanical properties of composite concrete. (a) Flexural stress–CMOD curves (the peaks represent the flexural strengths) for the C28 series (left) and C1 series (right). CX, gray curve; CX-R0, black curve; CX-N/H, red curve; CX-N, blue curve; CX-N/O. green curve; and CX-O, magenta curve. (b) Flexural strength, (c) fracture energy, and (d) compression strength of composite samples. C28 samples were cured for 28 days at room temperature and C1 samples were cured for 24 h at 85°C. CMOD, crack mouth opening displacement

TABLE 1 The observed transitions in the emission spectrum

Species	Transition	Wavelength (nm)
$N_2^+(1^-)$	$B^2\Sigma_u^+ \to X^2\Sigma_g^+$	391.1; 427.8; 470.9
$N_2 (2^+)$	$A^3\Sigma_u^+$	315.9
	$C^3\Pi_\mu \to B^2\Pi_g$	336.7; 357.6; 380.8
N–H	$A^3\Pi \to X^2\Sigma^-$	336.3
N–O	$A^2\Sigma^+ \to X^2\Pi$	247.0
O*	$3p^5P \to 3s^5S$	777.0
	$3p^3P \to 3s^3S$	844.0
		393.0; 436.0
H_α		656.3

TABLE 2 Results of roughness measurements

Samples	Roughness (μm)
R0	0.35 ± 0.03
N_2/O_2	0.4 ± 0.01
N_2	0.46 ± 0.02
O_2	0.93 ± 0.05
N_2/H_2	0.39 ± 0.01

of the untreated samples. The flexural strength and fracture energy values follow the same trend, with the N/O samples being the worst, and the other ones lower but comparable with the untreated one.

When considering the compression strength (Figure 6d), the gap between untreated and plasma-treated rubber is reduced. Additionally, the difference with respect to bare concrete remains significant. However, in both series (C28 and C1), an encouraging outcome was observed for N_2/H_2 plasma-treated rubber concrete (C28-N_2/H_2 and C1-N_2/H_2), with experimental values that are around 15% better than those of the reference composite.

In summary, it clearly emerges that plasma treatments under a reducing atmosphere (such as in the case of an N_2/H_2 plasma) significantly improve the mechanical performance of rubber concrete, probably due to the

TABLE 3 Results of mechanical tests for composite concrete samples

Samples	Flexural strength (MPa)[a]	Fracture energy (J/cm^2)[a]	Compression strength (MPa)[a]
C28	4.5 ± 0.6	4.6 ± 1.1	31.4 ± 6.0
C28-R0	2.7 ± 0.2	1.7 ± 0.1	13.6 ± 2.2
C28-N$_2$/O$_2$	2.6 ± 0.6	1.5 ± 0.4	14.2 ± 4.5
C28-N$_2$	3.4 ± 1.3	2.7 ± 0.6	13.9 ± 2.1
C28-O$_2$	2.9 ± 0.5	2.5 ± 0.7	11.6 ± 1.7
C28-N$_2$/H$_2$	3.2 ± 0.3	2.4 ± 0.2	15.7 ± 3.0
C1	4.6 ± 0.3	3.3 ± 0.4	35.8 ± 1.2
C1-R0	3.0 ± 0.8	2.9 ± 1.1	9.7 ± 2.5
C1-N$_2$/O$_2$	1.8 ± 0.7	1.9 ± 0.1	10.0 ± 2.3
C1-N$_2$	2.5 ± 0.6	2.5 ± 1.3	9.4 ± 0.8
C1-O$_2$	2.7 ± 0.7	2.9 ± 0.9	10.6 ± 1.3
C1-N$_2$/H$_2$	2.6 ± 0.1	2.6 ± 1.0	11.4 ± 1.3

[a]Values are averages of at least three measurements $\pm$ SD.

improved interfacial compatibility between rubber and the cement paste.

3.3 | Analysis of mechanical data for composite concrete

To provide a better understanding of the rubber concrete composites behavior, a scaling law was developed to highlight the parameters that most influence the mechanical performance.

The delamination and sliding friction of the rubber in a cement matrix can be modeled in a similar way to other composite aggregates. The main governing parameter is expected to be the fracture energy (or critical energy release rate) G_c, which can be modified through various plasma treatments. Scaling laws have been previously proposed for the strength and toughness dependence on G_c of materials subjected to fracture phenomena.[51,52] The strength dependence can be expressed as

$$\sigma \propto \sqrt{G_c}, \qquad (1)$$

so that we can expect the measured flexural strength σ to be proportional to the square root of G_c. The measured data of flexural strength versus fracture energy are plotted in Figure 7. Despite some scatter in the data, the fit provides an exponent of 0.6, close to the expected value of 0.5.

Two terms mainly contribute after plasma treatment to G_c: a chemical term G_f (related to the chemical links
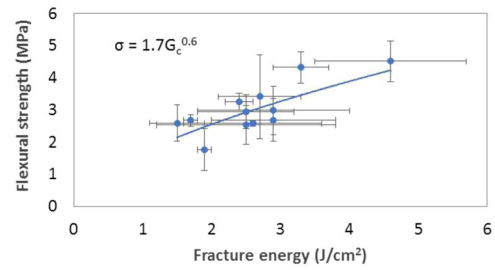

FIGURE 7 Measured flexural strength versus fracture energy for various plasma-treated samples (note that the 1.7 constant is not a pure number)
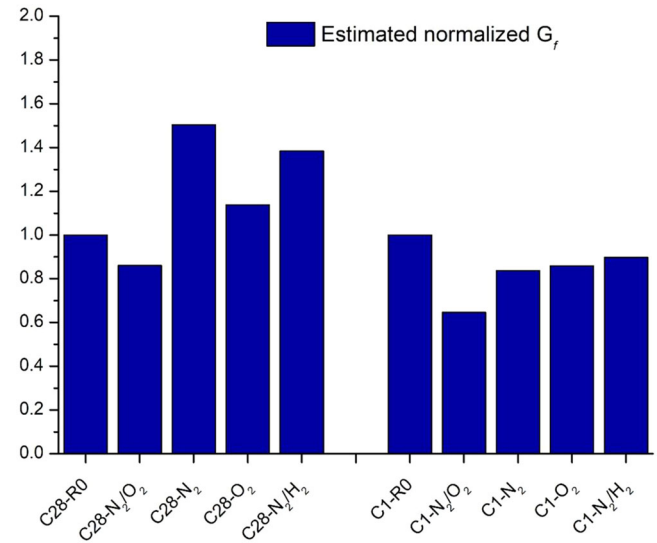

FIGURE 8 Estimated normalized G_f from the measured samples: plasma treatment may increase intrinsic adhesion

created between rubber and cement matrix), and a topological term (related to the roughness of the interface). This last term can be correlated to the qualitatively observed increase in roughness R_a of the plasma-treated surfaces and the simplest assumption is linearity. Thus, we can write G_c as

$$G_C = G_f(1 + R_a/R_{a_*}), \qquad (2)$$

where R_{a_*} is a characteristic roughness value, thus only a chemically-induced adhesive term $G_c = G_f$ is present for a perfectly flat surface ($R_a = 0$). Analyzing fracture energies G_c and relating them to measured roughness values R_a, the data appears to be rather scattered, with an overall variation that is of the order of the uncertainty on G_c values. Therefore, it is difficult to determine a deterministic value for R_{a_*} in Equation (2). However, we can estimate the intrinsic/chemical adhesive term as $G_f = G_c/(1 + R_a/R_{a_*})$ for the different samples. The normalized values with respect to the R0 sample value ($G_f/G_{f,R0}$), are presented in Figure 8 for both C1 and C28 samples

considering for R_{a_*} the best fit values respectively of 3.2 and 1.6 μm.

Regarding C28 samples, it is evident how N_2/H_2 and N_2 plasma treatments provide a significant improvement of the intrinsic adhesive term, while the N_2/O_2 treatment provides a slightly smaller adhesive term than the R0 one. The O_2 treatment does not significantly modify the intrinsic adhesive term, although in this case, the fracture energy increases substantially thanks to the roughness increment. In general, plasma treatment increases both roughness and intrinsic adhesion, thus the overall concrete fracture energy/toughness and strength.

Regarding C1 samples, all the composites containing plasma-treated rubber present smaller estimated G_f values than in the untreated case. The trend is somewhat similar to that of C28 samples, but the smaller G_f values confirm that the coupling of plasma treatment with a high-temperature cement curing is detrimental for the adhesion between cement and rubber.

4 | CONCLUSIONS

In this study, end-of-life rubber from waste tires was successfully included in concrete to partially replace the aggregate fraction. Two different cement matrices were compared: a Portland cement (C28), cured at room temperature and a Class G cement (C1), cured at 85°C. To favor the compatibility between the hydrophobic rubber and the hydrophilic cement matrix, plasma treatments have been performed on the rubber. In particular, the effects induced by four different plasma atmospheres (N_2/H_2, N_2, N_2/O_2, O_2) with different oxidizing capacities were compared.

The chemical modifications induced on rubber by the different plasma treatments were discussed, even if further characterization is needed to fully comprehend the chemical reaction pathways happening during the plasma treatments. Mechanical tests showed that C28 composites filled with plasma-treated rubber show an increment in terms of flexural strength, toughness/fracture energy, and slight compression strength if compared with the rubber concrete containing untreated rubber. These effects are more pronounced in the case of the N_2/H_2 plasma, whereas mechanical properties slightly deteriorate using an N_2/O_2 plasma. Interestingly, this rationalization is not valid in the case of C1 composites, where the performance of plasma-treated samples is generally worse than that of untreated rubber concrete. This phenomenon could be ascribed to the high temperature used for curing the C1 cement, which can affect the stability of the plasma-induced chemical modifications.

Undoubtedly, further work is required to reduce the performance gap with respect to bare concrete. However, plasma treatment is shown here to be a feasible alternative solution to standard chemical treatments to improve the interfacial compatibility between rubber and cement, thanks to improvements of both intrinsic adhesion and roughness of the interface and thus globally of the concrete strength and toughness, paving the way for future technological applications of rubber concrete.

ORCID

Luca Lavagna 🄳 http://orcid.org/0000-0003-3678-1366
Federico Bosia 🄳 http://orcid.org/0000-0002-2886-4519

REFERENCES

[1] K. B. Najim, M. R. Hall, *Constr. Build. Mater.* **2010**, *24*, 2043.
[2] G. Li, M. A. Stubblefield, G. Garrick, J. Eggers, C. Abadie, B. Huang, *Cem. Concr. Res.* **2004**, *34*, 2283.
[3] C. G. Papakonstantinou, M. J. Tobolski, *Cem. Concr. Res.* **2006**, *36*, 1686.
[4] J. Xue, M. Shinozuka, *Constr. Build. Mater.* **2013**, *42*, 196.
[5] A. O. Atahan, A. Ö. Yücel, *Constr. Build. Mater.* **2012**, *36*, 617.
[6] C. A. Issa, G. Salem, *Constr. Build. Mater.* **2013**, *42*, 48.
[7] K. B. Najim, M. R. Hall, *Mater. Struct.* **2013**, *46*, 2029.
[8] W. H. Yung, L. C. Yung, L. H. Hua, *Constr. Build. Mater.* **2013**, *41*, 665.
[9] N. Segre, I. Joekes, *Cem. Concr. Res.* **2000**, *30*, 1421.
[10] J. Lv, T. Zhou, Q. Du, H. Wu, *Constr. Build. Mater.* **2015**, *91*, 145.
[11] M. Geissdoerfer, P. Savaget, N. M. P. Bocken, E. J. Hultink, *J. Cleaner Prod.* **2017**, *143*, 757.
[12] R. Nisticò, *Resources* **2017**, *6*, 65.
[13] J. Claramunt, L. J. Fernández-Carrasco, H. Ventura, M. Ardanuy, *Constr. Build. Mater.* **2016**, *115*, 230.
[14] R. A. Sá Ribeiro, M. G. Sá Ribeiro, K. Sankar, W. M. Kriven, *Constr. Build. Mater.* **2016**, *123*, 501.
[15] E. Bonet-Martínez, L. Pérez-Villarejo, D. Eliche-Quesada, P. J. Sánchez-Soto, B. Carrasco-Hurtado, E. Castro-Galiano, *Mater. Lett.* **2018**, *229*, 21.
[16] H. P. S. Abdul Khalil, A. H. Bhat, A. F. Ireana Yusra, *Carbohydr. Polym.* **2012**, *87*, 963.
[17] A. Keskisaari, T. Kärki, *Resour., Conserv. Recycl.* **2018**, *134*, 257.
[18] A. Merlo, L. Lavagna, D. Suarez-Riera, M. Pavese, *Case Stud. Constr. Mater.* **2020**, *13*, e00467.
[19] R. Nisticò, P. Evon, L. Labonne, G. Vaca-Medina, E. Montoneri, C. Vaca-Garcia, M. Negre, *J. Cleaner Prod.* **2017**, *167*, 68.
[20] R. Nisticò, P. Evon, L. Labonne, G. Vaca-Medina, E. Montoneri, M. Francavilla, C. Vaca-Garcia, G. Magnacca, F. Franzoso, M. Negre, *ChemistrySelect* **2016**, *1*, 2354.

[21] F. Franzoso, C. Vaca-Garcia, A. Rouilly, P. Evon, E. Montoneri, P. Persico, R. Mendichi, R. Nisticò, M. Francavilla, *J. Appl. Polym. Sci.* **2016**, 133.

[22] X. Lin, J. Yu, H. Li, J. Y. K. Lam, K. Shih, I. M. L. Sham, C. K. Y. Leung, *J. Hazard. Mater.* **2018**, *357*, 40.

[23] R. Nisticò, L. Lavagna, D. Versaci, P. Ivanchenko, P. Benzi, *Boletín de la Sociedad Española de Cerámica y Vidrio* **2020**, *59*, 186.

[24] D. Suarez-Riera, A. Merlo, L. Lavagna, R. Nisticò, M. Pavese, *Boletín de la Sociedad Española de Cerámica y Vidrio* **2020**. in press.

[25] M. Sienkiewicz, J. Kucinska-Lipka, H. Janik, A. Balas, *Waste Manage.* **2012**, *32*, 1742.

[26] A. M. Rashad, *Int. J. Sustainable Built Environ.* **2016**, *5*, 46.

[27] V. Torretta, E. C. Rada, M. Ragazzi, E. Trulli, I. A. Istrate, L. I. Cioca, *Waste Manage.* **2015**, *45*, 152.

[28] European Tyre & Rubber Manufacture, statistical report 2011.

[29] N. I. Fattuhi, L. A. Clark, *Constr. Build. Mater.* **1996**, *10*, 229.

[30] S. Sgobba, M. Borsa, M. Molfetta, G. C. Marano, *Constr. Build. Mater.* **2015**, *98*, 820.

[31] X. Colom, J. Cañavate, F. Carrillo, J. I. Velasco, P. Pagès, R. Mujal, F. Nogués, *Eur. Polym. J.* **2006**, *42*, 2369.

[32] A. Meddah, M. Beddar, A. Bali, *J. Cleaner Prod.* **2014**, *72*, 187.

[33] L. Lavagna, R. Nisticò, M. Sarasso, M. Pavese, *Materials* **2020**, *13*, 1234.

[34] K. Bisht, P. V. Ramana, *Constr. Build. Mater.* **2017**, *155*, 811.

[35] A. Vesel, M. Mozetic, *J. Phys. D: Appl. Phys.* **2017**, *50*, 293001.

[36] R. Nisticò, G. Magnacca, S. Martorana, *Appl. Surf. Sci.* **2017**, *419*, 860.

[37] M. Moreno-Couranjou, P. Choquet, J. Guillot, H.-N. Migeon, *Plasma Processes Polym.* **2009**, *6*, S397.

[38] A. Zille, F. R. Oliveira, A. P. Souto, *Plasma Processes Polym.* **2015**, *12*, 98.

[39] P. Avetta, R. Nisticò, M. G. Faga, D. D'Angelo, E. A. Boot, R. Lamberti, S. Martorana, P. Calza, D. Fabbri, G. Magnacca, *J. Mater. Chem. B* **2014**, *2*, 5287.

[40] R. Nisticò, G. Magnacca, M. G. Faga, G. Gautier, D. D'Angelo, E. Ciancio, R. Lamberti, S. Martorana, *Appl. Surf. Sci.* **2013**, *279*, 285.

[41] R. Nisticò, M. G. Faga, G. Gautier, G. Magnacca, D. D'Angelo, E. Ciancio, G. Piacenza, R. Lamberti, S. Martorana, *Appl. Surf. Sci.* **2012**, *258*, 7889.

[42] P. Rivolo, R. Nisticò, F. Barone, M. G. Faga, D. Duraccio, S. Martorana, S. Ricciardi, G. Magnacca, *Mater. Sci. Eng., C* **2016**, *65*, 287.

[43] R. Nisticò, A. Rosellini, P. Rivolo, M. G. Faga, R. Lamberti, S. Martorana, M. Castellino, A. Virga, P. Mandracci, M. Malandrino, G. Magnacca, *Appl. Surf. Sci.* **2015**, *328*, 287.

[44] X. Zhang, X. Zhu, M. Liang, C. Lu, *J. Appl. Polym. Sci.* **2009**, *114*, 1118.

[45] I. Briata, Terni Energia S.p.A., Impianti PFU.

[46] L. Lavagna, S. Musso, G. Ferro, M. Pavese, *Cem. Concr. Compos.* **2018**, *88*, 165.

[47] L. Lavagna, D. Massella, E. Priola, M. Pavese, *Cem. Concr. Compos.* **2021**, *115*, 103851.

[48] G. Tillet, B. Boutevin, B. Ameduri, *Prog. Polym. Sci.* **2011**, *36*, 191.

[49] K. S. Suraj, P. Bharathi, V. Prahlad, S. Mukherjee, *Surf. Coat. Technol.* **2007**, *202*, 301.

[50] D. O. Hummel, In *Atlas of Plastics Additives: Analysis by Spectrometric Methods* (Ed: D. O. Hummel), Springer Berlin Heidelberg, Berlin, Heidelberg **2002**, p. 9.

[51] N. Pugno, A. Carpinteri, *J. Appl. Mech.* **2004**, *70*, 832.

[52] N. M. Pugno, *J. Mech. Phys. Solids* **2010**, *58*, 1397.